Conductivity and thermoelectric coefficients of doped SrTiO₃ at high temperatures

Kh. G. Nazaryan [1] and M. V. Feigel'man [2,1]

[1]*Moscow Institute of Physics and Technology, Dolgoprudny, Moscow Region 141700, Russia*
[2]*L.D. Landau Institute for Theoretical Physics, Chernogolovka, Moscow Region 143432, Russia*

We developed a theory of electric and thermoelectric conductivity of lightly doped SrTiO₃ in the nondegenerate region $k_B T \geqslant E_F$, assuming that the major source of electron scattering is their interaction with soft transverse optical phonons present due to proximity to ferroelectric transition. We have used the kinetic equation approach within relaxation-time parametrization of the collision integral and we have determined energy-dependent transport relaxation time $\tau(E)$ by the iterative procedure. Using electron effective mass m and electron-transverse phonon coupling constant λ as two fitting parameters, we are able to describe quantitatively a large set of the measured temperature dependences of resistivity $R(T)$ and Seebeck coefficient $\mathcal{S}(T)$ for a broad range of electron densities studied experimentally in recent paper by Collignon *et al.* [Phys. Rev. X **10**, 031025 (2020)]. In addition, we calculated Nernst ratio $\nu = N/B$ in the linear approximation over weak magnetic field in the same temperature range.

I. INTRODUCTION

Very dilute three-dimensional metal originating from band insulator strontium titanate (STO) due to tiny doping (10^{-6}–10^{-3} conduction electrons per unit cell) demonstrates a number of rather unusual properties [1–3]. Their major common origin is the close proximity of insulating STO to a ferroelectric transition, which leads to a giant low-temperature dielectric constant $\epsilon_0 \approx 20\,000$. In result, Coulomb interaction between conduction electrons is nearly vanishing, and standard phenomenology developed in the theory of normal metals is not applicable. The very low attainable density n of conduction electrons and its variability allow one to study transport properties of doped STO in various temperature regimes, from strongly degenerate Fermi gas at $k_B T \ll E_F$ to a highly nondegenerate one at $k_B T \gg E_F$, with E_F being the Fermi energy. The latter range is in the focus of recent experimental studies [4,5] (see also similar mobility data in Ref. [6] and thermoelectric data in Ref. [7]). It was found [5] that at high temperatures $T \geqslant 300\,\mathrm{K}$ conductivity drops below Mott-Ioffe-Regel limit and, moreover, relaxation rate $1/\tau$ becomes larger than its apparent quantum limit $k_B T/\hbar$. Later on, the paper [4] demonstrates that the account for the temperature-dependent renormalization of the effective mass $m(T)$ makes the above contradiction less drastic. However, the behavior of $m(T)$ found in Ref. [4] via the fitting of their data for resistance $R(T)$ and Seebeck coefficient $\mathcal{S}(T)$ is somewhat unexpected. Namely, mass renormalization $m(T)/m_0$ fitted in [4] depends not only on temperature but also on the electron density n, which should not be the case in the nondegenerate region $k_B T \gg E_F$ studied. Also, the initial increase on $m(T)$ with T growth is replaced by its drop with temperature at T above 300 K, which does not have a physical explanation.

In the present paper we reconsider theoretically the issue of electric conductivity and thermoelectric response in a nondegenerate electron gas, interacting with soft transverse optical (TO) phonons. These types of phonons exist in STO due to its proximity to ferroelectric transition [2–4,8]. Scattering of nondegenerate electrons due to biquadratic coupling to transverse optical phonons was considered in a somewhat different context in Refs. [9,10] (see also older experiments [11,12]). The recent paper [13] provided another approach to kinetic properties based upon the idea of the dominant role of electron scattering on two TO phonons; we will compare our results with those of Ref. [13] in the final part of the paper.

We use the kinetic equation approach in a form close to that discussed in Ref. [14] and express both resistivity $R(T)$ and Seebeck coefficient $\mathcal{S}(T)$ in terms of the energy-dependence transport scattering time $\tau(E, T)$. We emphasize that the energy dependence of $\tau(E, T)$ is not weak, and this is the reason why a simple proportionality relation [4] between Seebeck coefficient $\mathcal{S}(T)$ and thermodynamic entropy per electron $S(T)$ is not valid, actually. Indeed, $\mathcal{S}(T) = \frac{k_B}{e} S(T)$ follows once $\tau(E, T)$ can be replaced by energy-independent $\tau(T)$, as we will show below.

The real band structure of SrTiO₃ is rather complicated (see, e.g., [15]), and detailed calculation of transport coefficients is hardly possible without use of heavy numerical procedures based upon band-structure calculations. Some examples of the latter type of approach can be found in Refs. [16,17]. While Ref. [16] reported good agreement of computed high-T mobility with experimental data, the later Ref. [17] asserts that numerically exact band-structure calculation does overestimate mobility at high T by a factor close to 10, while providing correct T dependence. Paper [17] hints that the discrepancy originates from temperature-dependent polaron effect leading to the increase of effective

electron mass with temperature. The later paper [18] presents the results obtained by numerical implementation of this type of approach: strong polaron effects due to electron-phonon interactions were taken into account and good agreement with numerically obtained data on mobility was obtained. Moreover it was found that strong incoherent effects (demonstrated by broad electron spectral function) are developing at $T \sim$ 250–300 K.

We will accept the general idea of the importance of T-dependent mass renormalization and develop a semiquantitative theory based upon the simplest model of parabolic electronic spectrum $E(p) = p^2/2m$ with temperature-dependent effective mass $m = m(T)$. We believe that the proximity of STO to ferroelectric transition is the key feature of this material; most probably it is responsible for its anomalous properties, thus we feel it useful to consider the effects of electron interaction with TO phonons in somewhat more detail. Thus our approach is clearly an alternative to the one developed in Refs. [16,17] where coupling to high-energy longitudinal phonons (LO) was studied as a major source of electron scattering. We emphasize, to avoid any confusion, that in the whole temperature we consider, the temperature-dependent TO phonon gap $\hbar\omega_T(T) \ll k_B T$, this condition is well fulfilled up to 1000 K, as Fig. 6 of Ref. [4] demonstrates. At the same time, LO phonons have much higher energy gaps.

Our goal is to provide a simple model of electron scattering leading to reasonable agreement with the data in the high-temperature region $T \gg E_F(n)$ for both conductivity $\sigma(T)$, Seebeck coefficient $\mathcal{S}(T)$, and Nernst coefficient $\nu(T)$. We will show that a straightforward kinetic equation approach leads (once moderate mass renormalization, weakly T dependent at high temperatures, is taken into account) to good agreement with the data for $\sigma(T)$ and $\mathcal{S}(T)$ in a broad range of temperatures $100 < T < 700$ K and for a broad range of electron densities $1.4 \times 10^{17} \leqslant n \leqslant 3.5 \times 10^{20}$ cm^{-3}.

The rest of the paper is organized as follows: we formulate our model in Sec. II, then in Sec. III we derive a Boltzmann kinetic equation for electrons interacting quadratically with TO phonons, and expose the major points of its solution in terms of the effective relaxation time $\tau_{TO}(p)$. Next, in Sec. IV we discuss the calculation of electric conductivity and thermoelectric coefficients in terms of this effective relaxation time (Secs. IV A and IV B) and then present our final results and compare them with experimental data in Sec. IV C. Section V contains our conclusions.

II. FORMULATION OF THE MODEL

We are interested in the high-temperature region where quantum statistics of electrons is irrelevant and it is sufficient to consider each electron individually interacting with lattice phonons. The Hamiltonian of an electron coupled to transverse optical phonons is

$$H = \int d^3r \left[-\hbar^2 \frac{\psi^\dagger(\mathbf{r})\nabla^2\psi(\mathbf{r})}{2m(T)} + g\rho_m \psi^\dagger(\mathbf{r})\psi(\mathbf{r})\mathbf{u}^2(\mathbf{r}) \right],$$

(1)

where $\rho_m = 5.11$ g/cm^3 is the STO mass density, $\psi(\mathbf{r})$ is the electron annihilation operator, and $\mathbf{u}(\mathbf{r})$ is the atomic displacement field related to the optical transverse mode (TO), $\nabla \mathbf{u} = 0$. Dispersion of this mode is $\omega(k) = \sqrt{\omega_{TO}^2 + (sk)^2}$ where $s \approx 7.5 \times 10^5$ cm/s is the TO mode velocity [19] and ω_{TO} is the temperature-dependent gap which grows with temperature [4,8,20]; in particular, ω_{TO} varies between 5 and 18 meV when T grows from 100 to 800 K. Bilinear coupling (1) to transverse phonons was proposed recently as a possible mechanism for superconductivity in doped STO [21]; we develop this idea further in a separate publication [22]. Another possible type of electron's coupling to transverse TO phonons may contain a vector term of the type of $i(\psi^+\nabla\psi - \text{H.c.})\mathbf{u}$, but we will not consider its effects here.

Effective band mass of electrons depends [23] on their concentration at low temperatures in the degenerate region $T \ll E_F$; in particular, for zero-temperature mass $m(0)/m_0 \approx$ 1.8 for lowest concentrations $n \leqslant 10^{18}$ cm^{-3}, while at higher doping $n \geqslant 4 \times 10^{18}$ cm^{-3} the same ratio $m(0)/m_0 \approx 4$; here m_0 is the free-electron mass. However, at high temperatures $T \gtrsim 150$ K Hall mobility is n independent, as follows from the data present in Ref. [4]. The same is expected for the effective mass, which may however depend on temperature, for two different reasons. First, one is due to nonparabolic dispersion with decreasing effective curvature of $\xi(\mathbf{p})$ at large momenta $|\mathbf{p}|$ (see Fig. 3 in Ref. [15]): at high T carriers with energies much above the bottom of the band are most relevant, and effective mass seen in transport characteristics increases; moreover, at high temperatures the major contribution to transport is provided by the lowest band since at large $|\mathbf{p}|$ it provides the largest density of states. The second reason for the mass enhancement is the polaron effect due to coupling with TO phonons [18]. A special remark is in order concerning our use of a parabolic model of spectrum in the situation of a highly anisotropic band [15]. The point is that at high temperatures we consider, the scattering rate $1/\tau_{TO}$ is rather high, so electrons quickly forget the directions of their momenta, thus isotropic approximation looks acceptable, at least for the beginning. Below we will treat $m(T)$ as a phenomenological fitting function, common for all concentrations n.

The coupling constant g in Eq. (1) has a natural dimension Length^3/Time^2. We present it in the form

$$g = \lambda a^3 \omega_L^2,$$

(2)

where $a = 0.39$ nm is the STO lattice constant, $\hbar\omega_L \approx$ 100 meV is the highest energy gap of all longitudinal optical modes, and λ is some dimensionless constant, to be determined below from the fit of our theory to the data.

III. THE KINETIC EQUATION AND EFFECTIVE RELAXATION TIME

In this section we consider soft TO phonons as the major source of electron scattering. In addition we consider the role of usual acoustic phonons and demonstrate that their contribution to the scattering rate is much smaller and can be neglected in the first approximation.

A. Transverse optical phonons

We will study electric and thermoelectric transport in an electron system using the Boltzmann kinetic equation. To find the transport coefficients within linear response theory, we expand the distribution function as $f_p \approx n_p + \delta n_p$. Here, $n_p = [\exp(\beta \xi_p) + 1]^{-1}$ is the Fermi-Dirac distribution with $\beta = 1/T$, and $\xi_p = E(p) - \mu$ with the chemical potential μ. This helps to write the linearized Boltzmann equation in the presence of both electric field and temperature gradient:

$$\left(-e\mathbf{E} - \xi_{\mathbf{p}} \frac{\nabla_{\mathbf{r}} T}{T}\right) \cdot v_{\mathbf{p}} \frac{\partial n_p(\xi_{\mathbf{p}})}{\partial \xi_{\mathbf{p}}} = I_{\mathrm{TO}}\{\delta n_p\}, \qquad (3)$$

where $\mathbf{v}_{\mathbf{p}} = \partial \xi_{\mathbf{p}}/\partial \mathbf{p} = \mathbf{p}/m^*$ is the group velocity. An exact expression for the collision integral $I_{\mathrm{TO}}\{\delta n_p\}$ which describes electron scattering by two TO phonons is of the following form (for the derivation, see Appendix A):

$$\frac{1}{A} I_{\mathrm{TO}}\{\delta n_{\boldsymbol{p}}\}$$

$$= 2 \int_{\boldsymbol{k_1 k_2}} \frac{\delta(E_{p'} + E_{k_1} - E_p - E_{k_2})}{\omega(k_1)\omega(k_2)} (\delta n_{\boldsymbol{p}}[(N_{k_2} - N_{k_1})n_{p'} - (N_{k_1} + 1)N_{k_2}] + \delta n_{\boldsymbol{p'}}[n_p(N_{k_2} - N_{k_1}) + (N_{k_2} + 1)N_{k_1}])$$

$$+ \int_{\boldsymbol{k_1 k_2}} \frac{\delta(E_{p'} - E_{k_1} - E_p - E_{k_2})}{\omega(k_1)\omega(k_2)} \left(-\delta n_{\boldsymbol{p}}\left[N_{k_1}N_{k_2} + \left(1 + N_{k_2} + N_{k_1}\right)n_{p'}\right] + \delta n_{\boldsymbol{p'}}\left((N_{k_2} + 1)(N_{k_1} + 1) - n_p(1 + N_{k_2} + N_{k_1})\right)\right)$$

$$+ \int_{\boldsymbol{k_1 k_2}} \frac{\delta(E_{p'} + E_{k_1} - E_p + E_{k_2})}{\omega(k_1)\omega(k_2)} (\delta n_{\boldsymbol{p}}[(1 + N_{k_1} + N_{k_2})n_{p'} - (N_{k_1} + 1)(N_{k_2} + 1)] + \delta n_{\boldsymbol{p'}}[n_p(1 + N_{k_2} + N_{k_1}) + N_{k_2}N_{k_1}]),$$

$$(4)$$

where $N_k = [\exp(\beta \omega_k) - 1]^{-1}$ is the Bose-Einstein distribution for TO phonons, and $A = \frac{\pi}{2} g^2$. We use the shortcut notation for the integrals $\int_{\boldsymbol{k_1 k_2}} = \int_{\mathrm{BZ}} \frac{d^3 \boldsymbol{k_1} d^3 \boldsymbol{k_2}}{(2\pi)^6}$, where BZ stands for the first Brillouin zone (we take it in spherical approximation). Integration over momenta in Eq. (4) is carried out under the condition of conservation of the total momentum (we neglect umklapp processes). Conservation of the total energy is expressed in the explicit form in Eq. (4) by the delta functions; the forms of their arguments demonstrate that the first line corresponds to the scattering of an electron by the TO phonon, while second and third lines correspond to emission and absorption of two TO phonons, correspondingly.

Scattering processes change electron energy by the typical amount $\sim k_B T$ that is of the order of typical electron energy in the nondegenerate region $k_B T \gg E_F$ we consider here. Therefore the only way to proceed is to solve the kinetic equation (3),(4) numerically and to find nonequilibrium correction to the distribution function $\delta n_{\boldsymbol{p}}$ originating due to electric field $\mathbf{E}$ or temperature gradient ∇T. It is useful to present the result of such a computation in terms of some *effective* relaxation time $\tau_{\mathrm{TO}}(p, T)$ according to the definition below:

$$I_{\mathrm{TO}}\{\delta n_{\boldsymbol{p}}\} \approx -\frac{\delta n_{\boldsymbol{p}}}{\tau_{\mathrm{TO}}(p)}. \qquad (5)$$

Effective relaxation rate $\tau_{\mathrm{TO}}^{-1}(p; T)$ which provides the best approximation of the exact $I_{\mathrm{TO}}\{\delta n_{\boldsymbol{p}}\}$ by the form of Eq. (5), can be found by means of the iterative method, described in detail in Appendix C.

Briefly, it works as follows. First we note that in the linear regime over weak electric field E, modification of the electron distribution function can be written in the form [which follows by comparison between Eq. (3) and Eq. (5)]

$$\delta n_{\boldsymbol{p}} \approx e\, \tau_{\mathrm{TO}}(p) \cdot (\boldsymbol{v_p}, \mathbf{E}) \frac{\partial n_F(\xi_p)}{\partial \xi_p}. \qquad (6)$$

The form of Eq. (6) assumes it is possible to neglect temperature gradient $\nabla_r T$ while calculating $\delta n_{\boldsymbol{p}}$ and $\tau_{\mathrm{TO}}(p)$, and we check it *a posteriori* (see the end of Appendix C 2).

The only unknown function here is $\tau_{\mathrm{TO}} = \tau_{\mathrm{TO}}(|\boldsymbol{p}|)$. In the case of the degenerate Fermi-gas relevant momentum $p = p_F$ and we are left with just a single number τ for relaxation time. At high temperatures $T \gg E_F$ the situation is more complicated. Relaxation time $\tau_{\mathrm{TO}}(|\boldsymbol{p}|)$ appears to be a strong function of the electron energy. To find this function we start from the simplest trial with $\tau_{\mathrm{TO}}(p) = \tau_{\mathrm{TO}}$ independent of energy, and substitute the corresponding $\delta n_{\boldsymbol{p}}^{(0)}$ into the right-hand side of Eq. (4). The result is then represented in the form of Eq. (6) with somewhat different $\tau_{\mathrm{TO}}^{(1)}(p)$ which is now energy dependent. Then the process is repeated upon convergence (see Appendix C 2). We have found that the difference of the obtained $\tau_{\mathrm{TO}}^{(2)}(p)$ and $\tau_{\mathrm{TO}}^{(3)}(p)$ is already quite small, thus it is possible to use $\tau_{\mathrm{TO}}^{(3)}(p)$ as our final approximation for the relaxation rate. It is shown in Fig. 1(a) for a number of different temperatures. One can clearly see in Fig. 1(a) that the momentum dependence of scattering time $\tau_{\mathrm{TO}}(p)$ is not weak. This is why the Seebeck coefficient $\mathcal{S}(T)$ is not just proportional to the thermodynamic entropy per electron $S(T)$ as was supposed in the paper [4]. Instead, we will employ an approach provided in Ref. [14] where various transport coefficients were found in terms of effective energy-dependent relaxation rate $1/\tau(p)$. Note that our definition of effective relaxation time $\tau_{\mathrm{TO}}(p)$ is not *a priori* invariant with respect to different sources of nonequilibrium; one could imagine that electric field $\mathbf{E}$ and temperature gradient ∇T could lead to the solutions of Boltzmann equations which correspond to
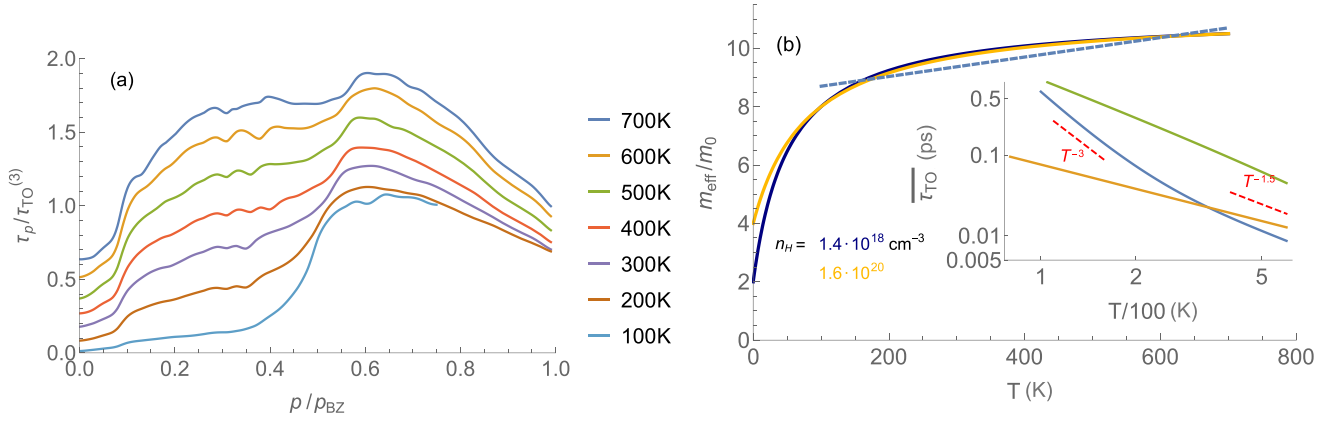
FIG. 1. (a) Lines represent the results of the third iteration of the iterative method for the inverse scattering time normalized to the inverse Planckian time $\tau_p/\tau_{TO}^{(3)}$. Here, $p_{BZ} = \hbar\pi/a$ stands for the first Brillouin zone and $\tau_p = \hbar/k_B T$. (b) Full lines show the expected qualitative temperature dependency of the effective mass. The dashed line stands for the linear dependency chosen in the present paper. The inset shows the comparison of the scattering time including two TO phonons averaged as $\overline{\tau_{TO}} = \langle \tau_{TO}\rangle/\langle 1\rangle$ (blue line), AC phonon (green line), and the Planckian time (orange line).

different $\tau_{TO}(p)$ functions. In fact, it is not the case, as we demonstrate in the Appendix C 2, the results for a "purely electric" source and for the case of zero-electric-current geometry, when electric field effect is completely compensated by the effect of thermal gradient, are very close to each other. It provides our effective relaxation time $\tau_{TO}(p)$ with more substantial physical meaning.

B. Acoustic phonons

The other mechanism that can probably contribute to the transport processes in the discussed temperature range is the scattering on the longitudinal acoustic (AC) phonons. The Hamiltonian of an electron coupling to an AC phonon reads

$$H_{ac} = \int D_{ac}\, \psi^\dagger(\mathbf{r})\psi(\mathbf{r})\, \mathrm{div}\, \mathbf{u}(\mathbf{r}), \tag{7}$$

where $\mathbf{u}(\mathbf{r})$ in this case is the atomic displacement field related to the acoustic mode. Their dispersion is given as $\omega(k) = v_s k$, with $v_s \approx 8.1 \times 10^5$ cm/s the sound velocity in STO [24]. The constant $D_{ac} \approx 2.87$ eV is the deformation potential in STO [25,26]. The interaction with the acoustic phonons results in a scattering time which can be approximated via the following expression [27]:

$$\tau_{AC} = \frac{(8\pi)^{1/2}\hbar^4 \rho_m v_s^2}{m^{3/2} D_{ac}^2 (k_B T)^{3/2}}. \tag{8}$$

This result is compared to the contribution from the scattering time on 2TO phonons [see the inset in Fig. 1(b)]. In the major part of the studied region the scattering rate due to TO phonons $1/\tau_{TO}$ turns out to be considerably greater than the acoustic phonon's contribution $1/\tau_{AC}$. Therefore, we may conclude that the consideration of only 2TO processes is an appropriate approximation, although for the temperatures at the lower end of the considered range the acoustic phonons can change the results slightly.

IV. TRANSPORT COEFFICIENTS IN TERMS OF EFFECTIVE RELAXATION TIME

A. Conductivity and Seebeck coefficient

Electric conductivity σ and the Seebeck coefficient $\mathcal{S}$ can be expressed via $\tau(p)$ as follows [14]:

$$\sigma = \frac{e^2}{m}\mathcal{N}\langle\tau_{TO}(p)\rangle, \tag{9}$$

$$\mathcal{S} = -\frac{1}{eT}\frac{\langle\xi_p \tau_{TO}(p)\rangle}{\langle\tau_{TO}(p)\rangle}, \tag{10}$$

where $\langle\cdots\rangle$ denotes the average $\langle X_p\rangle = -\frac{4}{3\mathcal{N}}\int_\mathbf{p} X_\mathbf{p}(\xi_\mathbf{p} + \mu)\frac{\partial n_p(\xi_\mathbf{p})}{\partial \xi_\mathbf{p}}$ with $\mathcal{N} = 2\int_p n_p(\xi_p)$. While Eq. (9) for conductivity is evident, the result (10) for the Seebeck coefficient needs some comments. Indeed, if one assumes $\tau(p)$ to be some constant (independent on p), then Eq. (10) leads to the relation $\mathcal{S}(T) = \frac{k_B}{e}S(T)$ used for the analysis developed in Ref. [4]. In fact, the p dependence of relaxation rate is very strong, as shown in Fig. 1(a).

Equations (9) and (10) can be derived as follows. We allow for the presence of both electric field $\mathbf{E}$ and temperature gradient ∇T and express $\delta n_\mathbf{p}$ using Eq. (3) for the collision integral in the relaxation-time approximation (RTA) form (5). The electric and thermal currents are then determined as follows:

$$\begin{pmatrix} \mathbf{J_E} \\ \mathbf{J}_T \end{pmatrix} = 2\int_\mathbf{p} \begin{pmatrix} -e \\ \xi_\mathbf{p} \end{pmatrix} \mathbf{v}_\mathbf{p}\delta n_\mathbf{p} = \begin{pmatrix} \sigma & \alpha \\ \beta & \kappa' \end{pmatrix}\begin{pmatrix} \mathbf{E} \\ -\nabla_\mathbf{r}T \end{pmatrix}, \tag{11}$$

where σ is electric conductivity, $\alpha = \beta/T$ due to Onsager reciprocity relations, and Seebeck coefficient $\mathcal{S} = \alpha/\sigma$. The use of $\delta n_\mathbf{p}$ in the form of Eq. (3) leads then to (9) and (10). Note that now we consider a kinetic equation in the presence of both electric field and temperature gradient; we checked in Appendix C 2 that the presence of ∇T does not change the function $\tau_{TO}(p)$ found previously.
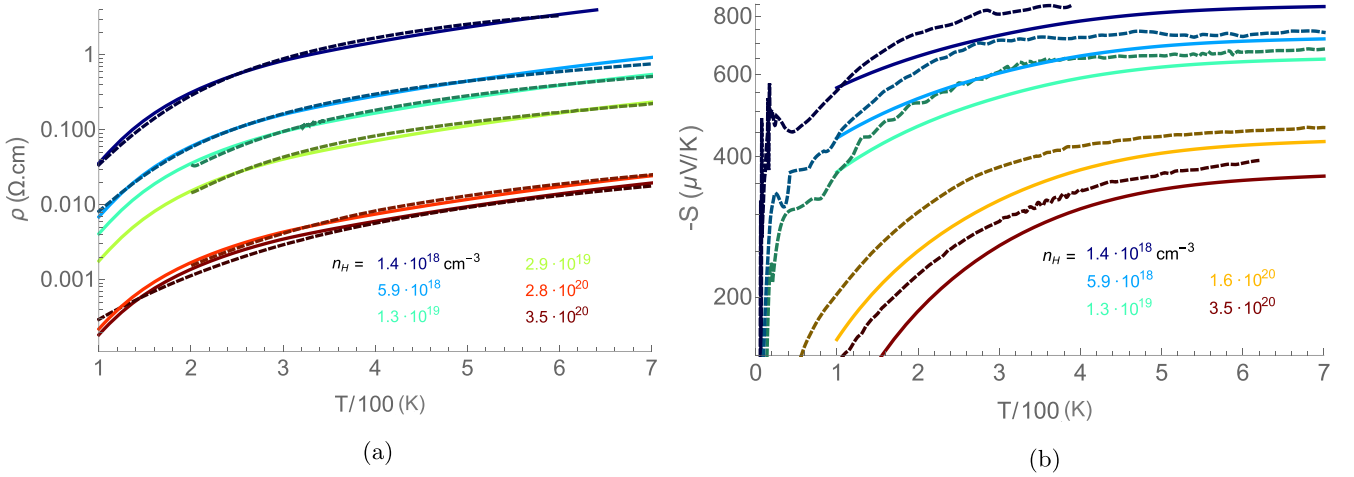
FIG. 2. Experimental data [4] are shown by dashed lines, while full lines are used for the theoretical results. (a) Temperature dependency of the resistivity extended to 700 K for several Nb doped SrTiO$_3$ crystals. (b) The Seebeck coecient as a function of temperature for four Nb doped SrTiO$_3$ samples from 100 K to 700 K.

B. Nernst coefficient

In the presence of magnetic field **B**, an applied electric field $\mathbf{E} \perp \mathbf{B}$ leads to the temperature gradient transverse to both **E** and **B**. The corresponding response is called Nernst signal, $N = E_y/\nabla_x T$. To calculate it we start from the general expression (see Sec. 5 of [28]) for N in terms of electric conductivity tensor $\sigma_{\alpha\beta}$ and thermoelectric tensor $\alpha_{\alpha\beta}$:

$$N = \frac{E_y}{\nabla_x T} = \frac{\alpha_{xy}\sigma_{xx} - \alpha_{xx}\sigma_{xy}}{\sigma_{xx}^2 + \sigma_{xy}^2}. \tag{12}$$

We concentrate here upon the limit of weak magnetic field and thus consider lowest-order terms in the magnitude of B:

$$\sigma_{xx} \approx \sigma; \quad \alpha_{xx} \approx \alpha = -\frac{e\mathcal{N}}{mT}\langle \xi_p \tau_{\text{TO}}(p)\rangle; \tag{13}$$

$$\sigma_{xy} \approx \frac{e^3\mathcal{N}}{m^2}B\langle \tau_{\text{TO}}^2(p)\rangle; \quad \alpha_{xy} \approx -\frac{e^2\mathcal{N}}{m^2 T}B\langle \xi_p \tau_{\text{TO}}^2(p)\rangle. \tag{14}$$

These equations lead us to the expression of the linear Nernst coefficient $\nu = dN/dB|_{B=0}$:

$$\nu = \frac{\langle \tau_{\text{TO}}^2(p)\rangle\langle \xi_{\mathbf{p}}\tau_{\text{TO}}(p)\rangle - \langle \tau_{\text{TO}}(p)\rangle\langle \xi_{\mathbf{p}}\tau_{\text{TO}}^2(p)\rangle}{T\langle \tau_{\text{TO}}(p)\rangle^2}. \tag{15}$$

Equation (15) will be used below to compute Nernst coefficient $\nu(T)$ as a function of temperature.

C. Results for the electric and thermoelectric coefficients

The obtained results for the scattering time τ_{TO} enabled calculation of the electric and thermoelectric coefficients using (9) and (10). The results of numerical computation for the electric resistivity and the Seebeck coefficient are provided in Figs. 2(a) and 2(b), respectively. The mass $m(T)$ and the coupling constant λ were fitted to experimental data from Ref. [4] in a way to minimize relative errors between the data and the theory. We emphasize that the single set of λ and $m(T)$ was used to fit the data for five different doping concentrations (apart from $n = 5.9 \times 10^{18}$ cm^{-3}), and relative error is about 7%–9%. Namely, we choose $\lambda = 0.88$ (with a

relative error of 5%) and effective mass $m(T)$ which linearly interpolates between $8.7m_0$ for 100 K to $10.7m_0$ for 700 K [see Fig. 1(b)]. For the concentration $n_H = 5.9 \times 10^{18}$ cm^{-3} we found $\lambda \approx 0.78$, which is almost 10% less than for the others.

Dependence of resistivity on temperature $\rho(T)$ in a broad temperature range cannot be present by any single power law. However, local "effective exponent" $\alpha(T)$ can be introduced via the relation $\alpha(T) = \frac{T}{\rho}\frac{d\rho}{dT}$. Our theoretic result for $\alpha(T)$ corresponding to the full curves in Fig. 2(a) is present in Fig. 3. Comparison with the data present in Fig. S1(a) of Ref. [4] shows excellent agreement for low electron concentrations; in particular, peculiarity of large $\alpha \approx 3$ in the temperature range 100–200 K is clearly reproduced by our theory, as well as the approach to a lower value of $\alpha \approx \frac{3}{2}$ at highest temperatures. At higher electron concentrations $n \geqslant 10^{20}$ the data [4] does not show so large values of $\alpha(T)$; this is due to the fact that the specific temperature range around 150 K lies below Fermi temperature $E_F(n)/k_B$, while our calculations were done for nondegenerate electrons only.

Our predictions for the Nernst coefficient $\nu(T)$ are shown in Fig. 4. We present our results for different electron densities but always for temperatures T above the corresponding Fermi energy $E_F(n)$. At these high temperatures $\nu(T)$ is independent
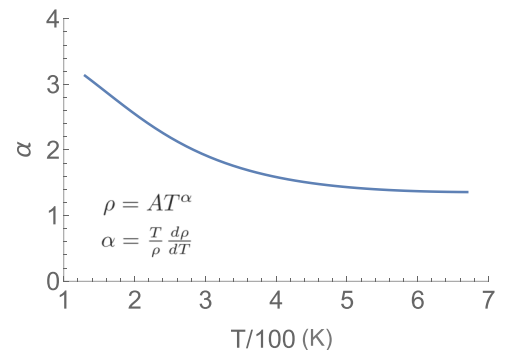
FIG. 3. Temperature dependency of the exponent α of the resistivity: $\rho = AT^\alpha$.
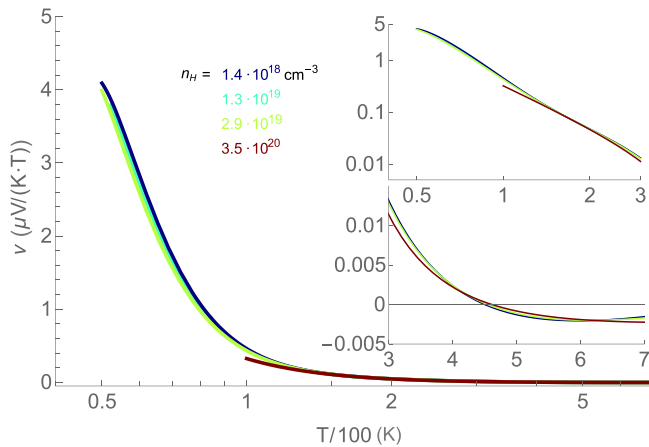
FIG. 4. Nernst coefficient $\nu(T)$ predicted for several Nb-doped SrTiO$_3$ samples from 50 to 700 K. The lower inset shows the temperature dependency of the Nernst coefficient in the range 300–700 K. The upper inset shows the same dependency from 50 to 300 K.

on the density of electrons, similar to the behavior of mobility $\mu(T)$. While at low temperatures the Nernst signal is known to be strongly n dependent [29], we are not aware of any measurement of this quantity in STO in the nondegenerate region $T \gg E_F$. The upper inset in Fig. 4 shows $\nu(T)$ in double-logarithmic scale, where one can infer a power-law-like behavior $\nu(T) \propto T^{-n}$ with $n \approx 3.5$. The lower inset is concentrated in the high-T region where a sign change of $\nu(T)$ is predicted at $T \approx 450$ K.

V. CONCLUSIONS

We developed a theory of conductivity and thermoelectric effects in doped strontium titanate in the nondegenerate region $T \gg E_F(n)$, assuming that the major source of electron scattering is due to processes which involve two soft optical (TO) phonons. The strength of the interaction between electrons and these TO phonons is determined by single dimensionless parameter λ. We have found good agreement between our theory and experiment [4] for both conductivity and Seebeck coefficient and for (almost) all electron concentrations, using a single value of $\lambda \approx 0.88$ and an assumption of an enhanced effective mass, with the ratio $m^*(T)/m_0$ varying between about 8.7 and 10.7 in the temperature interval 100–700 K (independent on n). A complementary study [22] of superconductivity in STO due to exchange by 2TO phonons produced very reasonable results with a similar value $\lambda = 1.1$ for the dimensionless coupling constant. Our kinetic equation approach correctly reproduces a temperature dependence of conductivity in various regions of moderate to high temperature. In particular, we obtained $\sigma(T) \propto T^{-3}$ behavior between about 100 and 200 K and slower dependence $\sigma(T) \propto T^{-3/2}$ at highest temperatures (see Fig. 3), in agreement with experimental data [4].

The major difference between our approach and the theory part of Ref. [4] is that we take into account energy dependence $1/\tau_{\mathrm{TO}}(p)$ which spoils simple proportionality between the Seebeck coefficient and entropy per particle. The same energy

dependence leads to a nonzero Nernst coefficient which we calculate in the linear approximation over magnetic field.

We have used the phenomenological notion of effective mass of electron, in spite of the fact that electron bands in STO are rather anisotropic (apart from the very bottom of the first band). Partial justification for the use of such approximation comes about since we consider a high-temperature nondegenerate region, where electrons frequently change their energy as well as momentum. An independent check for the value of the effective mass about $10m_0$ that we used comes from the analysis of the plasma frequency measurements [30]. Indeed, these data for electron density $n = 1.5 \times 10^{20}$ cm^{-3} show the drop of plasma frequency by the factor ~ 1.5 while temperature grows from 1 to 200 K. Using the relation $m(T) \propto 1/\omega_p^2(T)$ we conclude that effective mass grows by the factor ~ 2.2 in the same temperature range. Since low-temperature band mass is close to $4m_0$ for this electron density, we find $m_{\mathrm{eff}}(T \sim 200) \approx 9m_0$, in good agreement with the value we used in our main analysis.

With the values obtained for our fit parameters λ and $m(T)$, we find average scattering rate $\langle 1/\tau_{\mathrm{TO}} \rangle$ which is below, or at most, 20% higher, than the inverse Planckian time $k_B T/\hbar$ [see inset to Fig. 1(b)]. The energy-dependent relaxation time $\tau_{\mathrm{TO}}(p)$ never becomes less than 60% of the Planckian time, and is longer than it is in the major part of the data shown in Fig. 1(a). Therefore we expect that the use of the standard kinetic equation we employed is possible for the problem studied, although corrections to it may occur to be non-negligible at highest temperatures.

Note added. We recently became aware of the paper [13], which is devoted to the T dependence of conductivity in STO due to scattering by 2TO phonons. While the basic mechanism of electron scattering considered in [13] is the same as in our paper, it is treated in a quite different way. Namely, scattering by 2TO phonons is considered as *effectively elastic* electron scattering by "thermal disorder" produced by slow TO phonons. As a result, the electron scattering rate and resistivity are found to scale as T^2/E_0 at low temperatures $T \lesssim E_0$, where E_0 depends on the strength of the coupling to 2TO phonons (estimated as ≈ 200 K in Ref. [13]). In addition, the scattering rate they found is independent on the electron energy due to the approximation of a zero TO phonon gap employed. Both these features of the low-T results of Ref. [13] differ from our results as well as from experimental observations; we believe that their major problem is due to elastic approximation. However, at high temperature $T \gtrsim E_0$ they obtained $\sigma \propto T^{-3/2}$, via nontrivial solution beyond quasiparticle approximation. This result is in qualitative agreement with our highest-T results obtained within the kinetic equation approach; this coincidence seems to indicate that a breakdown of quasiparticle description due to $\hbar/T > \tau_{\mathrm{TO}}(p)$ does not lead to substantial consequences for conductivity.

ACKNOWLEDGMENTS
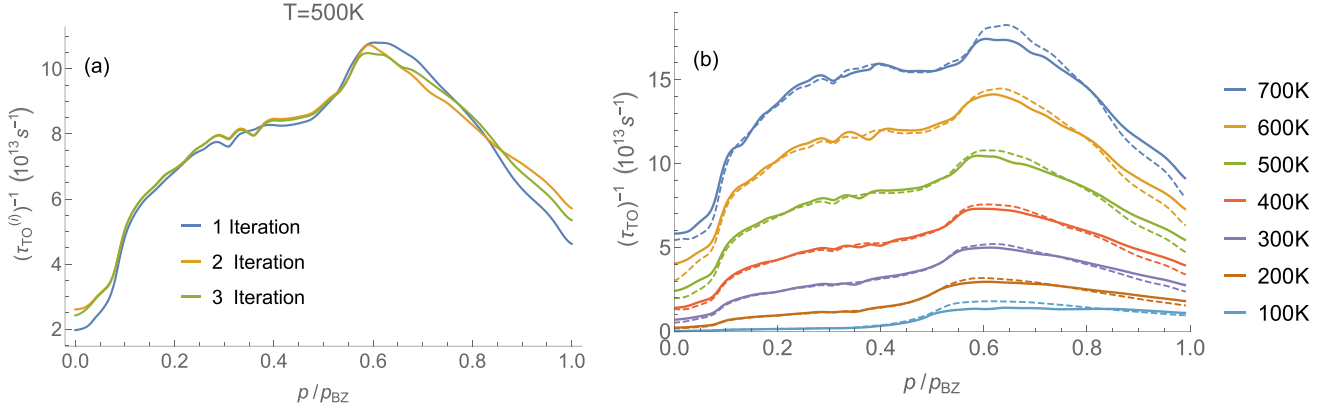
FIG. 5. These plots represent the results of the implemented iterative method. $p_{\mathrm{BZ}} = \hbar\pi/a$ stands for the first Brillouin zone. (a) The relaxation rate $1/\tau_{\mathrm{TO}}^{(i)}$ for $i = 1, 2, 3$ iterations for a fixed temperature $T = 500$ K. (b) The relaxation rates $1/\tau_{\mathrm{TO}}^{(i)}$ for $i = 1, 3$ iterations for the considered range of temperatures.

APPENDIX A: COLLISION INTEGRAL

In order to treat the Hamiltonian (1) we must represent the phonon operators in the second quantization form

$$\hat{\boldsymbol{u}}(\boldsymbol{r}) = \frac{1}{\sqrt{N}} \sum_{\boldsymbol{k},\lambda} \frac{\boldsymbol{e}_{\boldsymbol{k}}^{\lambda}}{\sqrt{2M\omega_{\boldsymbol{k}}}} \left(\hat{a}_{\boldsymbol{k}}^{\lambda} e^{-i\omega_{\boldsymbol{k}}t + i\boldsymbol{k}\boldsymbol{r}} + \text{e.c.}\right), \quad \text{(A1)}$$

where $\hat{a}_{\boldsymbol{k}}^{\lambda}$ is the phonon annihilation operator, M is the mass of the unit sell, N is the number of cells, and $\boldsymbol{e}_{\boldsymbol{k}}^{\lambda}$ is the λ polarization vector. This rewrites the Hamiltonian in a form

$$\hat{\mathcal{H}}_{\mathrm{TO}} = \frac{g}{2MN} \sum_{\boldsymbol{k}_1,\boldsymbol{k}_2,\lambda,\mu} \frac{\boldsymbol{e}_{\boldsymbol{k}_1}^{\lambda} \boldsymbol{e}_{\boldsymbol{k}_2}^{\mu}}{\sqrt{\omega_{\boldsymbol{k}_1}\omega_{\boldsymbol{k}_2}}} \left(\hat{\mathcal{F}}_{\boldsymbol{k}_1\boldsymbol{k}_2}^{(1)\lambda\mu} + \hat{\mathcal{F}}_{\boldsymbol{k}_1\boldsymbol{k}_2}^{(2)\lambda\mu}\right), \quad \text{(A2)}$$

$$\hat{\mathcal{F}}_{\boldsymbol{k}_1\boldsymbol{k}_2}^{(1)\lambda\mu} = \left(\hat{a}_{\boldsymbol{k}_1}^{\lambda} \hat{a}_{\boldsymbol{k}_2}^{\mu} e^{i(\boldsymbol{k}_1+\boldsymbol{k}_2)\boldsymbol{r}}\right) e^{-i(\omega_{\boldsymbol{k}_1}+\omega_{\boldsymbol{k}_2})t} + \text{e.c.}, \quad \text{(A3)}$$

$$\hat{\mathcal{F}}_{\boldsymbol{k}_1\boldsymbol{k}_2}^{(2)\lambda\mu} = \left(\hat{a}_{\boldsymbol{k}_1}^{\lambda} \hat{a}_{\boldsymbol{k}_2}^{\dagger\mu} e^{i(\boldsymbol{k}_1-\boldsymbol{k}_2)\boldsymbol{r}}\right) e^{-i(\omega_{\boldsymbol{k}_1}-\omega_{\boldsymbol{k}_2})t} + \text{e.c.} \quad \text{(A4)}$$

For the scattering probability we will use Fermi's golden rule. Here, each term in the Hamiltonian gets a simple physical interpretation. $\hat{\mathcal{F}}_{\boldsymbol{k}_1\boldsymbol{k}_2}^{(1)}$ will stand for the processes when two phonons are absorbed or emitted, and $\hat{\mathcal{F}}_{\boldsymbol{k}_1\boldsymbol{k}_2}^{(2)}$ for the process of scattering on a phonon.

Now, we take into account $\langle\langle\hat{\psi}_{\boldsymbol{p}}^{\dagger}\hat{\psi}_{\boldsymbol{p}}\rangle\rangle = f_{\boldsymbol{p}}$, $\langle\langle\hat{\psi}_{\boldsymbol{p}}\hat{\psi}_{\boldsymbol{p}}^{\dagger}\rangle\rangle = 1 - f_{\boldsymbol{p}}$, $\langle\langle\hat{a}_{\boldsymbol{k}}^{\dagger}\hat{a}_{\boldsymbol{k}}\rangle\rangle = N_{\boldsymbol{k}}$, $\langle\langle\hat{a}_{\boldsymbol{k}}\hat{a}_{\boldsymbol{k}}^{\dagger}\rangle\rangle = N_{\boldsymbol{k}} + 1$, where $\hat{\psi}_{\boldsymbol{p}}^{\dagger}$, $\hat{\psi}_{\boldsymbol{p}}$ are electron creation and annihilation operators, respectively, and $f_{\boldsymbol{p}}$ and $N_{\boldsymbol{k}}$ are nonequilibrium distributions for electrons and phonons, respectively. The last step is to represent the electron distribution function as follows, $f_{\boldsymbol{p}} \approx n_{\boldsymbol{p}} + \delta n_{\boldsymbol{p}}$, and take the phonon distribution to be almost equilibrium $N_{\boldsymbol{k}} \approx \mathcal{N}_{\boldsymbol{k}}$. Finally, the collision integral vanishes when all the distributions are taken to be the equilibrium ones. Therefore, by saving only the terms linear with respect to $\delta n_{\boldsymbol{p}}$ we end up with (4).

APPENDIX B: PARAMETRIZATION OF THE COLLISION INTEGRAL

The collision integral is of the form

$$I_{\mathrm{TO}}\{\delta n_{\boldsymbol{p}}\} = \int_{\boldsymbol{k}_1\boldsymbol{k}_2} f_1(k_1, k_2, p)\delta n_{\mathbf{p}} + f_2(k_1, k_2, p)\delta n_{\mathbf{p'}} \quad \text{(B1)}$$

where the functions f_1, f_2 were found in (4). The momentum p' is expressed via $\boldsymbol{k}_1, \boldsymbol{k}_2, \boldsymbol{p}$. Let us fix the function $\delta n_{\mathbf{p}}$. After the integration over $\boldsymbol{k}_1, \boldsymbol{k}_2$ we will get a function of the momentum p: $I_{\mathrm{TO}} \equiv I_{\mathrm{TO}}(\boldsymbol{p})$. Now, for that fixed $\delta n_{\mathbf{p}}$ we can introduce a function

$$\tau_{\mathrm{TO}}(p) = -\frac{\delta n_{\mathbf{p}}}{I_{\mathrm{TO}}(\mathbf{p})}. \quad \text{(B2)}$$

As a result we will have an exact parametrization of our collision integral in a form

$$I_{\mathrm{TO}}(\mathbf{p}) = -\frac{\delta n_{\mathbf{p}}}{\tau_{\mathrm{TO}}(p)}. \quad \text{(B3)}$$

The function $\tau_{\mathrm{TO}}(p)$ introduced in this way depends indeed on the function $\delta n_{\mathbf{p}}$ itself. But the physical problem presumes an existence of some source of deviation from the Fermi distribution which results from a certain external source (electric field, temperature gradient, etc.), which means that in every specific problem $\tau(p)$ can be determined. It is not guaranteed that the same $\tau(p)$ will be obtained for different types of perturbation.

Our method apparently looks similar to the RTA; however, in contrast to RTA, we do not make any approximations and use an exact parametrization of the collision integral. For the sake of simplicity, we call $\tau_{\mathrm{TO}}(p)$ *effective relaxation time*.

APPENDIX C: CALCULATION OF THE RELAXATION TIME

1. The iterative method

In order to find the relaxation time we assume that the temperature gradient in the Boltzmann equation can be
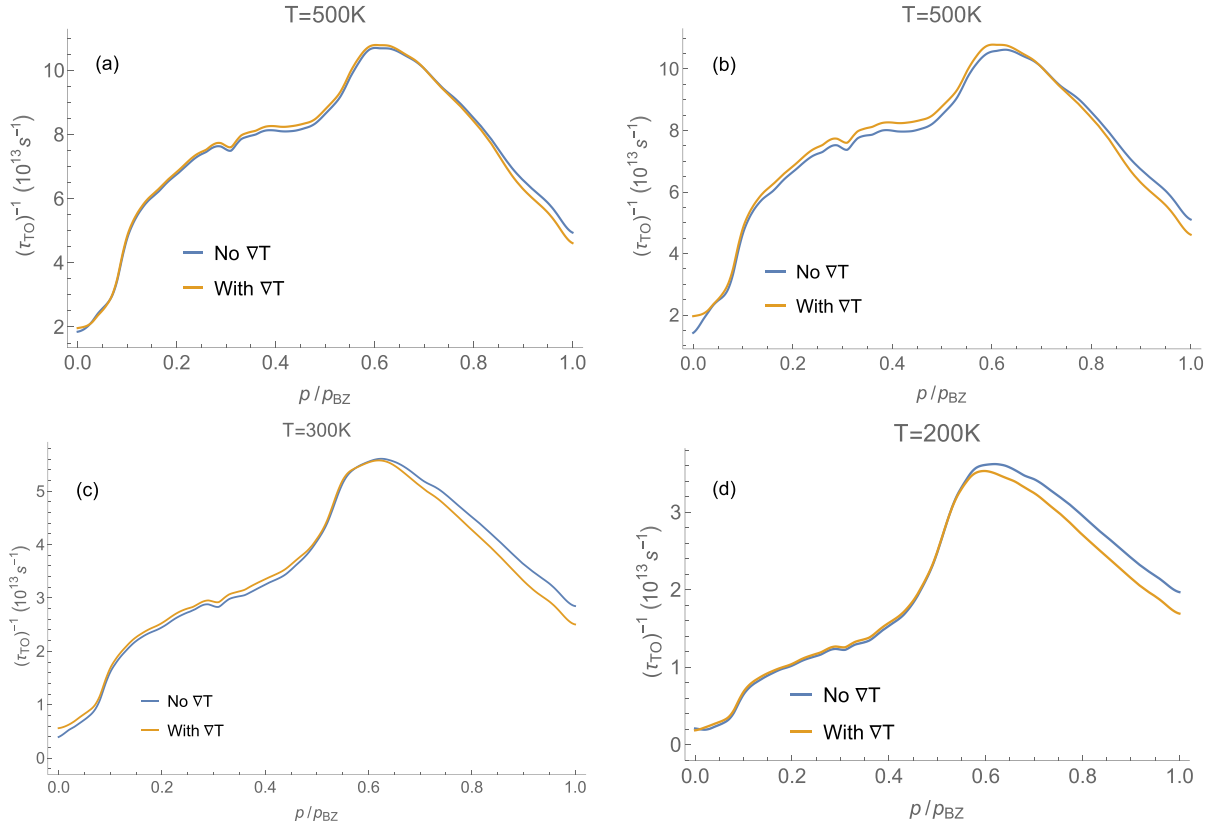
FIG. 6. The results for the relaxation time with and without the temperature gradient considered for two values of the Seebeck coefficient. (a) $\mathcal{S} = 700\,\mu\text{V/K}$. (b)–(d) $\mathcal{S} = 300\,\mu\text{V/K}$.

neglected. This assumption is checked in Appendix C 2. Therefore, we can rewrite the equation for $\delta n_{\boldsymbol{p}}$ in the following form:

$$\delta n_{\boldsymbol{p}} \approx e\tau_{\text{TO}}(p) \cdot (\boldsymbol{v_p}, \mathbf{E}) \frac{\partial n_F(\xi_p)}{\partial \xi_p}, \tag{C1}$$

$$I_{\text{TO}}\{\delta n_{\boldsymbol{p}}\} \equiv -\frac{\delta n_{\boldsymbol{p}}}{\tau_{\text{TO}}(p)}. \tag{C2}$$

Now, let us introduce our modification of the iterative method for this case.

Zeroth iteration. We start from the simplest trial with an energy-independent relaxation time:

$$\tau_{\text{TO}}^{(0)} = \text{const.} \tag{C3}$$

$$\delta n_{\boldsymbol{p}}^{(0)} \approx e\tau_{\text{TO}}^{(0)} \cdot (\boldsymbol{v_p}, \mathbf{E}) \frac{\partial n_F(\xi_p)}{\partial \xi_p}. \tag{C4}$$

First iteration. We substitute (C4) into (C2):

$$I_{\text{TO}}^{(1)}\{\delta n_{\boldsymbol{p}}^{(0)}\} = \text{Integral}\{\delta n_{\boldsymbol{p}}^{(0)}\} \equiv -\frac{\delta n_{\boldsymbol{p}}^{(0)}}{\tau_{\text{TO}}^{(1)}(p)}, \tag{C5}$$

$$\longrightarrow \tau_{\text{TO}}^{(1)}(p) = -\frac{\delta n_{\boldsymbol{p}}^{(0)}}{\text{Integral}\{\delta n_{\boldsymbol{p}}^{(0)}\}}, \tag{C6}$$

where the word "Integral" means that we numerically evaluate the integral in (4) using $\delta n_{\boldsymbol{p}}^{(0)}$ defined with (C4). Here, we know $\delta n_{\boldsymbol{p}}^{(0)}$ as a function of $\boldsymbol{p}$ to within the constant factor $\tau_{\text{TO}}^{(0)}$.

The key part is that $I_{\text{TO}}^{(1)}\{\delta n_{\boldsymbol{p}}^{(0)}\}$ is linear with respect to $\delta n_{\boldsymbol{p}}^{(0)}$, which means that the value of $\tau_{\text{TO}}^{(0)}$ cancels out from Eq. (C5). This allows us to extract $\tau_{\text{TO}}^{(1)}$. Using it, we find the modified distribution function

$$\delta n_{\boldsymbol{p}}^{(1)} \approx e\tau_{\text{TO}}^{(1)}(p) \cdot (\boldsymbol{v_p}, \mathbf{E}) \frac{\partial n_F(\xi_p)}{\partial \xi_p}. \tag{C7}$$

Second iteration. Similarly,

$$I_{\text{TO}}^{(2)}\{\delta n_{\boldsymbol{p}}^{(1)}\} = \text{Integral}\{\delta n_{\boldsymbol{p}}^{(1)}\} \equiv -\frac{\delta n_{\boldsymbol{p}}^{(1)}}{\tau_{\text{TO}}^{(2)}(p)}. \tag{C8}$$

Here, we already know $\delta n_{\boldsymbol{p}}^{(1)}$, so no problems in finding $\tau_{\text{TO}}^{(2)}$. And then

$$\delta n_{\boldsymbol{p}}^{(2)} \approx e\tau_{\text{TO}}^{(2)}(p) \cdot (\boldsymbol{v_p}, \mathbf{E}) \frac{\partial n_F(\xi_p)}{\partial \xi_p}. \tag{C9}$$

nth iteration.

$$I_{\text{TO}}^{(n)}\{\delta n_{\boldsymbol{p}}^{(n-1)}\} = \text{Integral}\{\delta n_{\boldsymbol{p}}^{(n-1)}\} \equiv -\frac{\delta n_{\boldsymbol{p}}^{(n-1)}}{\tau_{\text{TO}}^{(n)}(p)}, \tag{C10}$$

$$\delta n_{\boldsymbol{p}}^{(n)} \approx e\tau_{\text{TO}}^{(n)}(p) \cdot (\boldsymbol{v_p}, \mathbf{E}) \frac{\partial n_F(\xi_p)}{\partial \xi_p}. \tag{C11}$$

The convergence of the presented method cannot be guaranteed. However, we are working with a strictly positive function $\tau_{\text{TO}}(p) > 0$; hence it has a strictly positive average value which can be considered as the $\tau_{\text{TO}}^{(0)}$. So, we can think

of $\tau_{\text{TO}}(p)$ as $\tau_{\text{TO}}(p) = \overline{\tau_{\text{TO}}} + \Delta\tau_{\text{TO}}(p)$ and if $\Delta\tau_{\text{TO}}(p)$ is not much greater compared to $\overline{\tau_{\text{TO}}}$, the method should converge.

Now, let us prove that if the numerical evaluation shows that the method converges ($\lim_{n\to\infty} \tau_{\text{TO}}^{(n)} = \tau_{TO}^{(\infty)}$; $\lim_{n\to\infty} \delta n_p^{(n)} = \delta n_p^{(\infty)}$), we can guarantee that the obtained result is the solution for (C1) and (C2). The reason for this is that if we formally take a limit $n \to \infty$ in (C10) and (C11), we end up with

$$\delta n_{\boldsymbol{p}}^{(\infty)} \approx e\tau_{\text{TO}}^{(\infty)}(p) \cdot (\boldsymbol{v_p}, \mathbf{E}) \frac{\partial n_F(\xi_p)}{\partial \xi_p}, \qquad \text{(C12)}$$

$$I_{\text{TO}}\{\delta n_{\boldsymbol{p}}^{(\infty)}\} = \text{Integral}\{\delta n_{\boldsymbol{p}}^{(\infty)}\} \equiv -\frac{\delta n_{\boldsymbol{p}}^{(\infty)}}{\tau_{\text{TO}}^{(\infty)}}. \qquad \text{(C13)}$$

The above pair of equations is fully equivalent to Eqs. (C1) and (C2), which concludes our proof.

2. Results for $\tau_{\text{TO}}(p)$ and the role of temperature gradient

The results of the implemented method are presented in Fig. 5. It is clear that the method converges very decently, as the difference between the third approximation and the second one is already quite small. Therefore, it is sufficient to consider $\tau_{\text{TO}}^{(3)}(p)$ to be our final approximation for the relaxation time.

As is clear from Eq. (C1), we neglected the temperature gradient while developing the iterative method. Let us now check whether this approximation was appropriate. In order to do that we assume the absence of the charge current $\mathbf{J_E} = 0$ which gives a correlation between the electric field and the temperature gradient $\boldsymbol{\nabla} T = E/\mathcal{S}$. We consider several temperatures and two values of the Seebeck coefficient. Figure 6 shows the comparison between the relaxation times computed with and without the temperature gradient.

[1] A. Spinelli, M. A. Torija, C. Liu, C. Jan, and C. Leighton, Electronic transport in doped SrTiO₃: Conduction mechanisms and potential applications, Phys. Rev. B **81**, 155110 (2010).

[2] M. N. Gastiasoro, J. Ruhman, and R. M. Fernandes, Superconductivity in dilute SrTiO: A review, Ann. Phys. **417**, 168107 (2020).

[3] C. Collignon, X. Lin, C. W. Rischau, B. Fauqué, and K. Behnia, Metallicity and superconductivity in doped strontium titanate, Ann. Rev. Condens. Matter Phys. **10**, 25 (2019).

[4] C. Collignon, P. Bourges, B. Fauqué, and K. Behnia, Heavy Non-Degenerate Electrons in Doped Strontium Titanate, Phys. Rev. X **10**, 031025 (2020).

[5] X. Lin, C. W. Rischau, L. Buchauer *et al.*, Metallicity without quasi-particles in room-temperature strontium titanate, npj Quant. Mater. **2**, 41 (2017).

[6] A. Verma, A. P. Kajdos, T. A. Cain, S. Stemmer, and D. Jena, Intrinsic Mobility Limiting Mechanisms in Lanthanum-Doped Strontium Titanate, Phys. Rev. Lett. **112**, 216601 (2014).

[7] T. A. Cain, A. P. Kajdos, and S. Stemmer, La-doped SrTiO₃ films with large cryogenic thermoelectric power factors, Appl. Phys. Lett. **102**, 182101 (2013).

[8] Y. Yamada and G. Shirane, Neutron scattering and nature of the soft optical phonon in SrTiO₃, J. Phys. Soc. Jpn. **26**, 396 (1969).

[9] Yu. N. Epifanov, A. P. Levanyuk, and G. M. Levanyuk, Coupling effect of carriers and ferroelectric soft mode on the temperature dependence of their mobility, Fiz. Tverd. Tela **23**, 690 (1981).

[10] Yu. N. Epifanov, A. P. Levanyuk and G. M. Levanyuk, Interaction of carriers with to-phonons and electrical conductivity of ferroelectrics, Ferroelectrics **35**, 199 (1981).

[11] O. N. Tufte and P. W. Chapman, Electron Mobility in Semiconducting STO, Phys. Rev. **155**, 796 (1967).

[12] H. P. R. Frederikse and W. R. Hosler, Hall mobility in SrTiO₃, Phys. Rev. **161**, 822 (1967).

[13] A. Kumar, V. I. Yudson, and D. L. Maslov, Quasiparticle and Nonquasiparticle Transport in Doped Quantum Paraelectrics, Phys. Rev. Lett. **126**, 076601 (2021).

[14] W.-R. Lee, A. M. Finkel'stein, K. Michaeli, and G. Schwiete, Role of electron-electron collisions for charge and heat transport at intermediate temperatures, Phys. Rev. Research **2**, 013148 (2020).

[15] D. van der Marel, J. L. M. van Mechelen, and I. I. Mazin, Common Fermi-liquid origin of T^2 resistivity and superconductivity in n-type SrTiO₃, Phys. Rev. B **84**, 205111 (2011).

[16] B. Himmetoglu, A. Janotti, H. Peelaers, A. Alkauskas, and C. G. Van de Walle, First-principles study of the mobility of SrTiO₃, Phys. Rev. B **90**, 241204(R) (2014).

[17] J.-J. Zhou, O. Hellman, and M. Bernardi, Electron-Phonon Scattering in the Presence of Soft Modes and Electron Mobility in SrTiO₃ Perovskite from First Principles, Phys. Rev. Lett. **121**, 226603 (2018).

[18] J.-J. Zhou and M. Bernardi, Predicting charge transport in the presence of polarons: The beyond-quasiparticle regime in SrTiO₃, Phys. Rev. Research **1**, 033138 (2019).

[19] W. Rehwald, Anomalous ultrasonic attenuation at the 105°K transition in strontium titanate, Solid State Commun. **8**, 607 (1970).

[20] D. Bäuerle, D. Wagner, W. Wöhlecke, B. Dorner, and H. Kraxenberger, Soft modes in semiconducting SrTiO₃: II. The ferroelectric mode, Z. Phys. B: Condens. Matter **38**, 335 (1980).

[21] D. van der Marel, F. Barantani, and C. W. Rischau, Possible mechanism for superconductivity in doped SrTiO₃, Phys. Rev. Research **1**, 013003 (2019).

[22] D. Kiselev and M. Feigel'man, Theory of superconductivity due to Ngai's mechanism in lightly doped SrTiO₃, arXiv:2106.09530.

[23] X. Lin, G. Bridoux, A. Gourgout, G. Seyfarth, S. Krämer, M. Nardone, B. Fauqué, and K. Behnia, Critical Doping for the Onset of a Two-Band Superconducting Ground State in SrTiO$_{3-\delta}$, Phys. Rev. Lett. **112**, 207002 (2014).

[24] R. O. Bell and G. Rupprecht, Elastic constants of strontium titanate, Phys. Rev. **129**, 90 (1963)

[25] A. N. Morozovska, E. A. Eliseev, G. S. Svechnikov, and S. V. Kalinin, Nanoscale electromechanics of paraelectric materials with mobile charges: Size effects and nonlinearity of electromechanical response of SrTiO₃ films, Phys. Rev. B **84**, 045402 (2011).

[26] X. Lin, B. Fauqué, and K. Behnia, Scalable T^2 resistivity in a small single-component Fermi surface, Science **349**, 945 (2015).

[27] C. Hamaguchi, *Basic Semiconductor Physics*, 2nd ed. (Springer, New York, 2010).

[28] K. Behnia, *Fundamentals of Thermoelectricity* (Oxford University Press, New York, 2019).

[29] X. Lin, Z. Zhu, B. Fauqué, and K. Behnia, Fermi Surface of the Most Dilute Superconductor, Phys. Rev. X **3**, 021002 (2013).

[30] J. L. M. van Mechelen, D. van der Marel, C. Grimaldi, A. B. Kuzmenko, N. P. Armitage, N. Reyren, H. Hagemann, and I. I. Mazin, Electron-Phonon Interaction and Charge Carrier Mass Enhancement in $SrTiO_3$, Phys. Rev. Lett. **100**, 226403 (2008).